

A hemodynamic correlate of lateralized visual short-term memories

Simone Cutini^a, Fabio Scarpa^a, Pietro Scatturin^a, Pierre Jolicœur^b, Patrik Pluchino^a,
Marco Zorzi^{c,d}, Roberto Dell'Acqua^{a,d,*}

^a Department of Developmental Psychology, University of Padova, Padova, Italy

^b Department of Psychology, University of Montreal, Montreal, Canada

^c Department of General Psychology, University of Padova, Padova, Italy

^d Centre for Cognitive and Brain Science, University of Padova, Padova, Italy

ARTICLE INFO

Article history:

Received 23 July 2010

Received in revised form

27 November 2010

Accepted 6 December 2010

Available online 14 December 2010

Keywords:

Visual short-term memory

Functional near-infrared spectroscopy

Intra-parietal sulcus

ABSTRACT

Neuroimaging studies attempting to isolate the neural substrate of visual short-term memory in humans have concentrated on the behavior of neurons populating the posterior part of the parietal cortex as a possible source of visual short-term memory capacity limits. Using a standard change-detection task, fMRI studies have shown that maintenance of bilaterally encoded objects elicited bilateral increases of hemodynamic activation in the intra-parietal and intra-occipital sulci (IPS–IOS) proportional to the number of objects retained in visual short-term memory. We used a spatially cued variant of the change-detection task to record hemodynamic responses to unilaterally encoded objects using functional near-infrared spectroscopy (fNIRS). Electrophysiological studies that employed this task have shown that maintenance of unilaterally encoded objects elicited posterior unilateral (contralateral) increase in event-related negativity proportional to the number of objects retained in visual short-term memory. We therefore examined whether contralateral increases in oxy-hemoglobin concentration correlated with the number of retained objects. Contrary to the idea that bilateral increases in BOLD responses and unilateral increases in event-related negativity may be different reflections of the same underlying neural/functional processing, memory-related increases in oxy-hemoglobin concentration were found bilaterally even when objects had to be encoded unilaterally. The present findings suggest that EEG and fMRI/fNIRS techniques reveal distinct neural signatures of the mechanisms supporting visual short-term memory.

© 2010 Elsevier Ltd. All rights reserved.

1. Introduction

Despite the extensive cortical structures specialized for vision (e.g., Zeki, 1993) and widely distributed cortical networks involved in visual short-term memory (VSTM; e.g., Cohen et al., 1997), our internal representation of the visual world is surprisingly sparse (Rensink, 2000a,b). It includes just a minuscule fraction of the information physically available for visual inspection. Behavioral investigations have converged to an estimate of VSTM capacity of just 3–4 objects (Cowan, 2001; Irwin, Brown, & Sun, 1988; Luck & Vogel, 1997; Rouder et al., 2008; Wheeler & Treisman, 2002). Although neurons showing sustained activation during the retention of VSTM objects populate a number of cortical regions of the human brain, including areas of the frontal and prefrontal cortex (Cohen et al., 1997; Courtney, Ungerleider, Keil, & Haxby, 1997; Nee & Jonides, 2009; Pessoa, Gutierrez, Bandettini, & Ungerleider,

2002), recent neurophysiological investigations have concentrated on an interesting property of neurons in posterior, parieto-occipital, regions that makes them particularly important *vis-à-vis* the issue of VSTM storage limits. Differently from neurons in other cortical areas, fMRI studies have revealed that blood oxygen level dependent (BOLD) responses recorded in posterior parietal regions tend to increase with the number of objects encoded in VSTM, but only up to VSTM capacity, leveling-off thereafter (Beck, Rees, Frith, & Lavie, 2001; Harrison, Jolicœur, & Marois, 2010; Robitaille et al., 2010; Todd & Marois, 2004; Xu & Chun, 2006).

Todd and Marois (2004), for instance, monitored the activity of neurons in the entire brain using fMRI and they looked for neurons with activity levels that increased with increasing memory load and reached a plateau in activity when memory performance also reached a plateau. They found such neurons in the intra-parietal sulcus (IPS) and intra-occipital sulcus (IOS) during the retention interval of a change-detection task. In this task, a memory array of objects must be compared with a probe array of objects presented shortly afterwards for detection of a change affecting a single object. The interval elapsing between memory and probe arrays was long enough that the task could not be performed on the basis of sensory persistence (Coltheart, 1980; Phillips, 1974) triggered by the

* Corresponding author at: Centre for Cognitive and Brain Science, Via Venezia 8, 35131 Padova, Italy. Tel.: +39 049 8276545; fax: +39 049 8276511.

E-mail address: dar@unipd.it (R. Dell'Acqua).

URL: <http://colab.psy.unipd.it> (R. Dell'Acqua).

objects shown in the memory array. It is assumed that encoded objects must be maintained in VSTM for successful performance in this task (Vogel, Woodman, & Luck, 2001). During the retention interval, the BOLD response elicited by the activity of IPS–IOS neurons correlated with VSTM load, showing a signal increase as the number of to-be-memorized objects was increased from one to four objects. No further increase in the BOLD response was observed when the number of to-be-memorized objects exceeded VSTM capacity, suggesting that processing in this brain region is severely capacity limited, or receives input from a capacity-limited system. Importantly, IPS–IOS neurons were shown to be insensitive to perceptual load (the total number of items shown), because the BOLD response elicited by an array of objects displayed in a simple detection task, which was designed to impose minimal requirement on VSTM resources, was unaffected by variations in the number of objects displayed (but see Mitchell & Cusak, 2008, for divergent findings).

Extensive explorations of the neural reflections of VSTM storage have also been conducted using a variant of the change-detection task and the event-related potential (ERP) approach. In this variant, the memory array is preceded by a centrally displayed arrow cue that points to the side of the screen from which participants encode visual objects that must be committed to memory. Objects on the other side must be ignored. ERPs recorded during the retention of lateralized objects have been shown to be more negative at posterior electrode sites over brain regions contralateral to the side of presentation of the remembered objects than at electrode sites over ipsilateral brain regions (Klaver, Talsma, Wijers, Heinze, & Mulder, 1999). This particular ERP response, labeled sustained posterior contralateral negativity (SPCN) by some (Jolicœur, Brisson, & Robitaille, 2008; Luria, Sessa, Gotler, Jolicœur, & Dell'Acqua, 2009), or contralateral delayed activity (CDA) by others (Vogel & Machizawa, 2004; Vogel, McCollough, & Machizawa, 2005), increases in amplitude as the number of items to be remembered is increased, but only up to VSTM capacity, leveling-off thereafter. Furthermore, SPCN variations modulated by memory load can predict individual differences in VSTM capacity (Vogel & Machizawa, 2004). These results make a strong case for a functional interpretation of the SPCN as a neurophysiological index of retention in VSTM that has been corroborated in a number of recent studies (Dell'Acqua, Sessa, Jolicœur, & Robitaille, 2006; Ikkay, McCollough, & Vogel, 2010; Jolicœur, Sessa, Dell'Acqua, & Robitaille, 2006; Jolicœur, Sessa, DelLeRobitaille, Grimault, & Jolicœur, 2009; Lefebvre, Jolicœur, & Dell'Acqua, 2010; Luria et al., 2009; McCollough, Machizawa, & Vogel, 2007; Perron et al., 2009; Predovan et al., 2009; Prime, Dell'Acqua, Arguin, Gosselin, & Jolicœur, 2010; Prime & Jolicœur, 2009; Robitaille, Grimault, & Jolicœur, 2009; Thériault, De Beaumont, Tremblay, Lassonde, & Jolicœur, 2010).

The isomorphism between memory-related BOLD responses recorded at IPS–IOS and the SPCN component of the ERP suggests that IPS–IOS neurons are part of the neural circuitry responsible for VSTM capacity limits. It is difficult to establish this functional interpretation with brain imaging methods, however, because of the general correlational nature of the measures. One could imagine, for example, that IPS–IOS neuronal activity reflects not the capacity limits of VSTM, *per se*, but rather some other constraint correlated with memory capacity, such as a limit in attentional mechanisms, or perhaps a limit imposed by capacity-limited mechanisms implemented in the frontal cortex (e.g., Johnson, Spencer, Luck, & Schöner, 2009). Alternatively, perhaps the behavior of IPS–IOS is not specific to VSTM, but rather is a reflection of a general memory constraint that is independent of sensory modality (Saults & Cowan, 2007).

Another important consideration is that early visual processing in striate areas is retinotopically organized. The retinotopic orga-

nization becomes coarser but still generally preserved as visual processing continues in higher-level, extra-striate visual areas (Aguirre, Zarahn, & D'Esposito, 1998; Jack et al., 2007; Zeki, 1993). At the coarsest level, the left and right halves of visual space are contralaterally represented in distinct cerebral hemispheres. The contralateral organization of the visual space seems to be generally retained in the lower portion of the dorsal visual stream up to and including the intra-parietal sulcus (IPS; Sereno, Pitzalis, & Martinez, 2001), and in inferior regions of the temporal cortex (Chelazzi, Miller, Duncan, & Desimone, 1993). The fact, therefore, that SPCN activity manifests itself as increased negative activity recorded at sites contralateral to the side of to-be-memorized information conforms nicely to the spatial organization of the visual information processed by IPS–IOS neurons. Crucially, to our knowledge, only one study has reported enhanced BOLD responses in posterior parietal regions contralateral to the side of presentation of lateralized to-be-memorized visual objects (Robitaille et al., 2010). In this study, larger load effects were found contralaterally to encoding side of visual stimuli for EEG and MEG results, with a clear plateau at VSTM capacity. This result, however, was not found for the BOLD response, for the same subjects, tested in fMRI in very similar paradigms. The BOLD response was larger in contralateral IOS/IPS than in ipsilateral cortex, but this difference did not plateau when memory could no longer hold more items. Interestingly, an earlier report by Robitaille et al. (2009) suggested that, although MEG revealed a larger contralateral load effect, during the retention of visual stimuli, there was also a strong load-dependent ipsilateral response. Robitaille et al. concluded that this pattern of response was more likely to be associated with perceptual or attentional mechanisms than with mechanisms of VSTM, *per se*.

Scope of the present work was to further explore the intriguing dissociation between the EEG results and those from fMRI and MEG suggested by the results of Robitaille et al. (2010), i.e., the only study so far that to our knowledge has employed the cued variant of the change-detection task with the concomitant recording of hemodynamic activity. To determine whether the increase in BOLD response associated with increases in VSTM load is larger in contralateral cortex, or differs in other ways from the ipsilateral response, we used the cued variant of the change-detection task and the functional near-infrared spectroscopy (fNIRS) technique to estimate the hemodynamic response recorded at the same regions of interest (ROIs) explored by Todd and Marois (2004) and others (e.g., Harrison et al., 2010; Robitaille et al., 2010; Song & Jiang, 2006; Xu & Chun, 2006). Similarly to fMRI, fNIRS permits measurements of local, functionally related, hemodynamic changes in the brain (e.g., Villringer, Planck, Hock, Schleinkofer, & Dirnagl, 1993). Unlike fMRI, however, which records signals based on the paramagnetic properties of deoxy-hemoglobin (HbR), fNIRS detects changes in the optical properties of the cortical surface mediated by variations in local hemodynamic activity. The method can estimate variations in the concentration of both HbR and oxy-hemoglobin (HbO). The sum of HbR and HbO concentrations provides an estimate of total blood volume (HbT) in a circumscribed brain region. In addition to providing an estimate of HbO (which cannot be estimated with fMRI), fNIRS systems can sample the changes in HbO and HbR concentration at a higher temporal resolution than is typically used in fMRI, which could potentially provide a more detailed picture of the dynamics of cortical activations during the execution of various cognitive tasks. These theoretical comparisons of fMRI and fNIRS have recently been confirmed by an influential fMRI–fNIRS co-registration study (Huppert, Hoge, Diamond, Franceschini, & Boas, 2006), showing that BOLD response is highly correlated with HbR concentration ($r = .98$), less correlated with HbO concentration ($r = .71$), and least correlated with HbT concentration ($r = .53$). However, HbR variations detected with fNIRS are well known to be characterized by a poorer signal-to-noise ratio with respect to HbO

and HbT variations (Strangman, Culver, Thompson, & Boas, 2002; Yamamoto & Kato, 2002), and the activation-signal amplitude of HbR is usually halved under the same stimulation circumstances relative to that of HbO (Maki, Yamashita, Watanabe, & Koizumi, 1996; Sato, Kiguchi, Kawaguchi, & Maki, 2004).

In summary, in the present work we used fNIRS to study brain responses produced by changes in VSTM load, and particularly to examine whether VSTM load effects elicited by unilaterally encoded stimuli were themselves lateralized to the contralateral portion of the posterior parietal cortex, and magnified with respect to possible VSTM load effects detected ipsilaterally to the visual hemifield including the to-be-memorized objects.

2. Experiment

2.1. Method

2.1.1. Participants

Thirteen right-handed students at the University of Padova (6 females, mean age 23.4 years \pm 2.8) participated after providing informed consent. All had normal or corrected-to-normal vision, and normal color vision. No participant reported a prior history of neurological or psychiatric disorder, and none was under medication at the time of testing.

2.1.2. Stimuli, design, and procedure

The stimuli were equiluminant (40 cd/m²) colored squares with a side of 1° of visual angle at a distance of 60 cm, that were displayed on a black (7 cd/m²) background on a cathode-ray tube monitor controlled by a microcomputer running MEL 2.0 Software. The colors were yellow, red, blue, green, white, cyan, orange, and violet. The colored squares occupied random positions within two rectangular regions of the screen, one to the left and one to the right of the center of the screen, that measured 3.5° (width) \times 7.0° (height), with the constraint that the distance between the centers of two adjacent squares could be no shorter than 2°. The distance between the inner boundary of each rectangular region and the center of the screen measured 0.8°.

The experiment was conducted in a sound-attenuated and dimly lit room. A schematic illustration of the sequence of events on a typical trial is shown in Fig. 1. Each trial started with the presentation of a plus sign at the center of the screen for 2 s. The plus sign was then replaced by a small circle (0.4°) for 600 ms, alerting participants to the upcoming presentation of the first (memory) array of colored squares. The alerting circle, which remained on the screen throughout the entire trial, was then flanked by an arrow head pointing to the left or to the right side of the screen, for 400 ms. The offset of the arrow head was followed by a 300 ms blank interval, and then by the presentation of the memory array, which remained visible for 300 ms. The memory array was composed of either four or eight colored squares, evenly distributed to the left/right of fixation (i.e., either two on each side, or four on each side). The squares were always of different colors. Following the memory array offset, a 1400–1600 ms blank interval, jittered randomly in steps of 20 ms, elapsed before the presentation of the second (probe) array of colored squares, that were displayed in the same positions as those occupied by the squares displayed in the memory array. The probe array remained in view until a response was detected (see below), or for a maximum duration of 3 s.

Participants were instructed to maintain their gaze at fixation, and memorize the color of the squares on the side of the memory array cued by the arrow head. They were informed that, on a random half of the trials, the color of one of the squares would change between the memory and probe arrays. Following the onset of the probe array, participants had to press, without speed pressure, one of two appropriately labeled keys of the computer keyboard to indicate whether a change in color had occurred or not. Following the response, or after a maximum of 3 s without a response, a 10–14 s intertrial interval (jittered randomly in steps of 500 ms) elapsed before the presentation of the plus sign for the next trial, which was replaced by a minus sign in case of an incorrect or undetected response on the previous trial, in order to provide ongoing feedback to participants about their performance. Trials were organized in 6 blocks of 24 trials (with a short pause between blocks). In each block, each combination of response (target present vs. target absent), number of to-be-memorized squares (2 vs. 4), and stimulus side (left vs. right) was equiprobable and the trial order within each block was randomized at run-time for each participant.

2.1.3. fNIRS apparatus and data acquisition

The recording optical unit was a multi-channel frequency-domain NIR spectrometer (ISS ImagentTM, Champaign, Illinois), equipped with 28 laser diodes (14 emitting light at 690 nm, and 14 at 830 nm) modulated at 110.0 MHz. The diode-emitted light was conveyed to the participant's head by multimode core glass optical fibers (heretofore, sources; OFS Furukawa LOWOH series) with a length of 250 cm and a core diameter of 400 μ m. Light that scattered through the brain and exiting the head was collected by detector optical fiber bundles (3 mm of diameter)

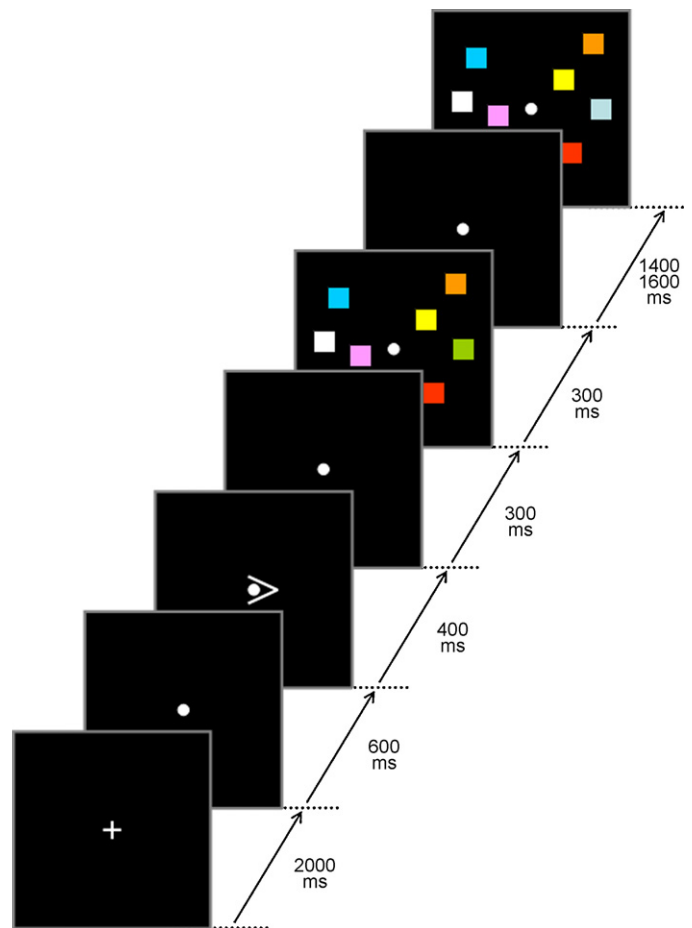


Fig. 1. Sequence of visual events on a typical trial of the present change-detection task (see text for details).

to 4 photo-multiplier tubes (PMTs; R928 Hamamatsu Photonics). The PMTs were modulated at 110.005 MHz, generating a 5.0 KHz heterodyning (cross-correlation) frequency. To separate the light as a function of source location, the sources time-shared the 4 parallel PMTs via an electronic multiplexing device. Only two sources (one per hemisphere) were synchronously ($t=4$ ms) active (i.e., emitting light), resulting in a final sampling period of 128 ms ($f=10^3/128=7.8125$ Hz) after dual-period averaging. Following detection and amplification by the PMTs, the optical signal was converted into temporal variations (Δ) of oxy-hemoglobin (Δ HbO) and deoxy-hemoglobin (Δ HbR) concentration. These values are known to depend on age (Schroeter, Zysset, Kruggel, & von Cramon, 2003), and were therefore corrected for the differential-pathlength factor (DPF; Cope & Delpy, 1988) using the equations described by Duncan et al. (1996):

$$\text{DPF}_{\text{HbO}} = 5.13 + 0.07 \times (\text{age})^{0.81} \quad (1)$$

$$\text{DPF}_{\text{HbR}} = 5.13 + 0.07 \times (\text{age})^{0.81} \quad (2)$$

Horizontal EOG (HEOG) was recorded bipolarly from tin electrodes positioned on the outer canthi of both eyes, referenced to the left earlobe. HEOG and right earlobe electrical activity were amplified and band-passed at 0.01–80 Hz using a Grass CP122 AC/DC amplifier. HEOG signal was conveyed to an auxiliary channel of the fNIRS apparatus and sampled at 7.8125 Hz (i.e., the sampling frequency of the fNIRS). Impedance at each electrode was maintained below 5 K Ω . HEOG activity was re-referenced offline to the average of the left and right earlobes, and segmented into baseline-corrected 1200 ms epochs starting 200 ms prior to the onset of arrow head until the offset of the memory array.

2.1.4. fNIRS probe placement procedure

Sources and detectors were held in place on the scalp using a custom-made holder and velcro straps. Each source was composed of two source optical fibers, one for each wavelength. The distance between each source/detector pair (heretofore, channel) was $L=30.0$ mm, so as to equate channels for optical penetration depth into the cortical tissue (about 20 mm; see Franceschini, Toronov, Filiaci, Gratton, & Fantini, 2000). The position of each channel coincided with the 20 mm cerebral projection of the midpoint of the source-detector distance. This probe arrangement included 18 channels, providing 18 measurements for HbO and 18 for HbR.

Table 1
Results of ipsilateral vs. baseline and contralateral vs. baseline comparisons for both concentration indices. From left to right: left/right labels of each symmetrical channel, MNI coordinates of the channels (negative *x* coordinates for the left hemisphere and positive *x* coordinates for the right hemisphere), corresponding Brodmann areas, and *z*-scores of Δ HbO and Δ HbT.

Ch.	MNI coordinates	Region	BA	Ipsilateral vs. baseline (z scores)		Contralateral vs. baseline (z scores)	
				HbO	HbT	HbO	HbT
A1/C1	–28 –62 70 29 –60 71	L/R sIPS	7	2.16	2.01	2.51	2.60
A2/C2	–39 –59 64 37 –58 63	L/R sIPS	7	2.38	2.16	1.98	1.90
A3/C3	–43 –67 54 41 –68 55	L/R ANG	39	1.82	2.03	1.95	1.94
A4/C4	–37 –75 52 39 –76 51	L/R IPS	7	1.95	1.90	2.23	1.98
A5/C5	–25 –76 58 27 –74 60	L/R pSPL	7	2.09	2.07	1.93	1.91
B3/D3	–46 –74 39 47 –73 40	L/R ANG	39	1.97	1.73	2.10	1.84
B4/D4	–38 –81 38 37 –82 38	L/R IPS–IOS	19	2.69	2.10	2.52	2.17
B6/D6	–51 –74 23 51 –73 24	L/R LOC	19	1.67	n.s.	1.69	n.s.
B7/D7	–38 –86 24 37 –85 23	L/R SOC	19	2.17	2.03	2.29	2.29

The spatial arrangement of source/detector pairs on the scalp was determined using a new probe placement approach (Cutini et al., 2010), based on the combined use of a physical model of the head surface of the ICBM152 template (ICBM152-PM) and a 3D neuronavigation software (Brain Sight™, RogueResearch). The stereotaxic coordinates of the cerebral ROIs investigated in the present experimental context overlapped with the ROIs reported in the fMRI studies of Todd and Marois (2004) and Xu and Chun (2006). Starting from these stereotaxic coordinates, the procedure developed by Cutini et al. (2010) was used to achieve a consistent, standardized positioning of the fNIRS channels on the scalp of each participant, so as to target the chosen stereotaxic coordinates based on those fMRI results. The procedure comprised the following three steps.

The 3D neuronavigation system was first used to individuate on the head surface of the ICBM152-PM template the projections of the target ROIs and estimate the MNI coordinates of the channels on the ICBM152 brain template, digitizing the midpoints of each source/detector pair with a cortical penetration depth of 20 mm and the head surface points of sources and detectors. The MNI coordinates and corresponding Brodmann areas of the channels are reported in Tables 1 and 2.

The channels were then anatomically labeled using a probabilistic atlas (Brede Database, <http://neuro.imm.dtu.dk/services/jerne/brede>). The sources on each hemisphere were numbered from 1 to 7. Left-hemisphere detectors were indicated with the letters A/B, and right-hemisphere detectors with the letters C/D. Channels A1/C1 and A2/C2 recorded activity from the superior IPS (sIPS), A3/C3 from

the angular gyrus (ANG), A4/C4 from the IPS, A5/C5 from the posterior part of the superior parietal lobule (pSPL), B3/D3 from the ANG, B4/D4 from the region at the intersection between IPS and IOS, B6/D6 from regions adjacent to the lateral occipital cortex (LOC), and B7/D7 from the superior occipital cortex (SOC). The resulting spatial arrangement of sources and detectors on the head surface is illustrated in Fig. 2a. The channels overlaid onto the ICBM152 brain template are illustrated in Fig. 2b. Both Fig. 2a and 2b were generated after remapping the stereotaxic points onto the ICBM152 template using MRICron (<http://www.sph.sc.edu/comd/rorden/mricron/>; for details, see Cutini et al., 2008).

The standardization across participants of the probe placement was finally achieved by relying on the bidirectional correspondence between 10–10 points (Nuwer et al., 1998) and the MNI coordinates of their cerebral projections (Okamoto et al., 2004). Three 10–10 reference points for each hemisphere were selected as landmarks, namely, Pz for both hemispheres, PO3/P5 for the left hemisphere, and PO4/P6 for the right hemisphere. The spatial arrangement of each set of landmarks generated a well-defined and consistent spatial binding that allowed us to standardize the probe placement across participants. The pair of '5'-sources was positioned symmetrically 1.5 cm below and left/right of Pz. The midpoint between '4'-sources and '7'-sources coincided with PO3 and PO4, respectively. Left-hemisphere and right-hemisphere '6'-sources coincided with P5 and P6, respectively. The degree of precision achieved with this procedure is comparable with that obtained using different approaches (Okamoto et al., 2004; Singh, Okamoto, Dan, Jurcak, & Dan,

Table 2
Results of load-2 condition vs. baseline and load-4 condition vs. baseline comparisons for both concentration indices. From left to right: left/right labels of each symmetrical channel, MNI coordinates of the channels (negative *x* coordinates for the left hemisphere and positive *x* coordinates for the right hemisphere), corresponding Brodmann areas, and *z*-scores of Δ HbO and Δ HbT.

Ch.	MNI coordinates	Region	BA	Load-2 vs. baseline (z scores)		Load-4 vs. baseline (z scores)	
				HbO	HbT	HbO	HbT
A1/C1	–28 –62 70 29 –60 71	L/R sIPS	7	2.26	2.19	2.49	2.36
A2/C2	–39 –59 64 37 –58 63	L/R sIPS	7	2.15	2.06	2.18	1.86
A3/C3	–43 –67 54 41 –68 55	L/R ANG	39	1.71	1.89	1.80	1.83
A4/C4	–37 –75 52 39 –76 51	L/R IPS	7	1.83	1.80	1.99	1.83
A5/C5	–25 –76 58 27 –74 60	L/R pSPL	7	1.95	2.01	2.16	2.04
B3/D3	–46 –74 39 47 –73 40	L/R ANG	39	1.85	n.s.	2.12	1.80
B4/D4	–38 –81 38 37 –82 38	L/R IPS–IOS	19	2.42	1.85	2.47	2.15
B6/D6	–51 –74 23 51 –73 24	L/R LOC	19	1.69	n.s.	1.63	n.s.
B7/D7	–38 –86 24 37 –85 23	L/R SOC	19	2.27	2.18	1.95	1.97

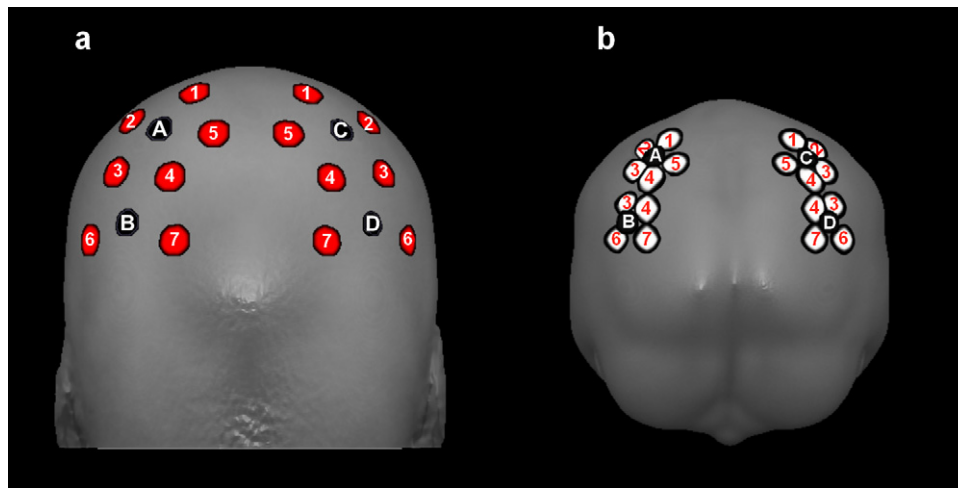


Fig. 2. Probe placement on the ICBM152 template (occipital view). (a) Sources (red circles) and detectors (black circles) overlaid on the head surface of the ICBM152-PM template; (b) Cerebral projections of sources (white circles) and detectors (black circles) overlaid on the ICBM152 brain template.

2005), yielding a worst-case average error that is below the spatial resolution of the present fNIRS setup.

2.1.5. fNIRS data processing and analysis

All the computations described in this section were performed using a custom software written in Matlab R2008b (The Mathworks, Natick, MA, USA) and details of the algorithms employed for data preprocessing and signal estimation can be found in Scarpa et al. (2010). Individual hemodynamic responses were segmented into 15 s trials starting from the onset of the memory array. Trials associated with an incorrect response and/or with an HEOG amplitude exceeding $\pm 30 \mu\text{V}$ during the interval from the onset of the arrow cue presentation and the offset of the memory array (8%) were discarded from analysis.

Trials were first divided into the four cells of the present experimental design generated by the orthogonal combination of the factors load (2 vs. 4 to-be-memorized colored squares displayed in the cued visual hemifield; hereafter, load-2 and load-4) and side (to-be-memorized colored squares displayed ipsilaterally vs. contralaterally relative to a given recording channels; hereafter, ipsilateral and contralateral, see below for further details). A sequence of operations was then performed for each subject, channel and condition. The optical signal of each trial was zero-mean corrected by subtracting the mean signal intensity recorded during the 15 s period from signal value sampled during the 15 s period. This procedure was adopted to reduce the impact of low-frequency physiological noise on the signal averaged across trials. Two algorithms were then applied for artifact removal. First, a custom procedure based on Grubbs' (1969) test was separately applied on the dataset in each condition. An artifact rejection threshold was set to the mean concentration value at a given sampling time-point ± 2.5 SDs. Trials with one or more values exceeding the Grubbs' threshold were discarded from analysis (1%). The remaining trials were successively filtered using the outlier removal algorithm proposed by Devaraj (2005), which considers variations in concentration of the hemodynamic signal throughout the entire trial rather than considering single time-points as the Grubbs' test. The mean value and the difference between the maximum and minimum values (range) were calculated considering all trials in a given condition. The mean value and range were also calculated for each single trial. Single-trial mean and range values were then compared with the mean values of all trials in that condition. Trials characterized by a range or mean value greater than the condition mean ± 2.5 SDs were discarded from analysis (2%). Signal averaging of all remaining trials in each condition was then performed. Noisy channels (with $\text{SD} > 800 \text{ nM}$) were discarded from analysis (1.1%). The averaged hemodynamic signal was smoothed with a Savitzky and Golay's (1964) filter with polynomial order equal to 3 and frame size equal to 25 time-points (i.e., 3.2 s). The resulting signal was baseline-corrected by subtracting the mean signal intensity in the 0–500 ms interval from the onset of the memory array from the averaged hemodynamic signal.

A first series of exploratory fNIRS data analyses was carried out to pinpoint the hemodynamic responses separately in the ipsilateral, contralateral, load-2 and load-4 conditions against baseline activity. In these analyses, mean ΔHbO and ΔHbR signal intensities during vascular response in a 6.5–8.5 s interval post memory-array display were calculated for each subject and condition. In order to perform an analysis similar to that usually conducted in ERP investigations of lateralized VSTM, each channel of one hemisphere was pooled with its symmetrical one of the other hemisphere (e.g., A3 with C3). For each symmetrical channel pair, ΔHbO and ΔHbR concentration values contralateral to the cued hemifield were calculated by averaging data recorded at left-sided channels when the to-be-memorized colored squares were displayed in the right visual hemifield and data recorded at right-sided channels when the to-be-memorized colored squares were displayed in the left visual

hemifield. Ipsilateral ΔHbO and ΔHbR concentration indices were calculated with an analogous algorithm by averaging data at the complementary channels. The same calculations were performed for the load-2 and load-4 conditions. By repeating the same procedures for each pair of channels, we obtained three individual optical maps (ΔHbO , ΔHbR , and ΔHbT) for each condition. The optical maps were analyzed (via one-tail *t*-tests) to identify the channels showing a significant activation increase relative to baseline for each concentration index and condition.

A second set of analyses capitalized on the higher sampling frequency of fNIRS (relative to fMRI) so as to produce per-subject estimates of the latency at which the hemodynamic response reached its peak value and relative response amplitude. To do so, the time at which the individual hemodynamic response reached the maximum value in the 0–10 s temporal window following the onset of the memory array was calculated. Peak latency was then used to derive the amplitude of individual hemodynamic response by calculating the mean value of the hemodynamic concentration in a 2 s time-window centered on peak latency. A set of individual optical maps in the contralateral condition and a set of individual optical maps in ipsilateral condition were generated based on the hemodynamic concentrations obtained with the individual peak-based approach. The two sets of maps were compared via *t*-tests to isolate the ROIs associated with a distinguishable lateralized hemodynamic response. The ROIs showing such a response were further examined for the presence of joint effects of side and load manipulations, predicted on the hypothesis of increased memory load effects in the hemisphere contralateral to the side of presentation of the to-be-encoded objects. All *t*-tests conducted on the concentration values were corrected for multiple comparisons using the false discovery rate method of Benjamini and Hochberg (1995; FDR_{BH}). The *q* value specifying the maximum FDR was set to .1, such that no more than 10% false positive could be included, on average, in the set of significantly active channels. In the fNIRS analyses, significant *t* values were converted into *z* scores to create *z*-maps. The *z* score of each channel pair was mapped onto an overlay map (1 mm^3 voxel size) at the correspondent midpoint expressed in MNI coordinates using the Nifti toolbox (Neuroimaging Informatics Technology Initiative, <http://www.nifti.nih.gov>). A Gaussian blurring filter ($\text{SD} = 10 \text{ mm}$) was applied to the overlay map to approximate the area covered by each channel. The resulting *z*-map was overlaid onto the ICBM152 brain template using MRICron Software.

2.2. Results

Data from two participants were discarded from analysis, in one case for behavioral performance not distinguishable from chance, and in the other case for problems with the fNIRS apparatus that occurred during data recording. All analyses described in the forthcoming paragraphs were carried out on data from the remaining eleven participants.

2.2.1. Behavior

The individual proportions of correct responses were submitted to analysis of variance (ANOVA) considering load and side as within-subject factors. The analysis revealed a less accurate performance in the load-4 condition (.79) than in the load-2 condition (.95; $F(1, 10) = 72.6$; $p < .001$). The factor side and interaction between side and load were not significant ($F_s < 1$). Individual

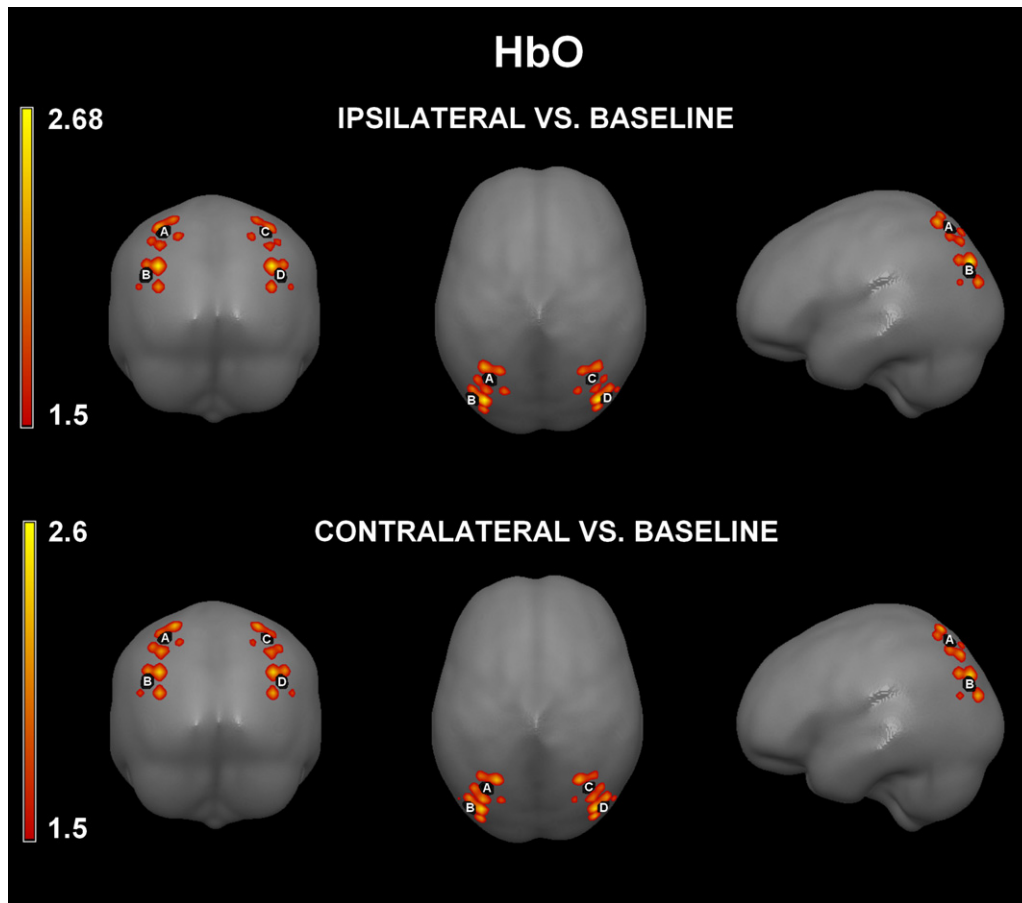


Fig. 3. Statistical (z) Δ HbO maps of the ipsilateral vs. baseline comparison (upper panels) and contralateral vs. baseline comparison (lower panels). From left to right: occipital view, top view and left temporal view. The z -maps have been overlaid onto the ICBM152 brain template.

Cowan's (2001) K indices were calculated separately for each load condition (load-2: $K = 1.79$; load-4: $K = 2.31$). These values differed significantly ($F(1, 10) = 11.2$; $p < .01$). An ANOVA considering the same factors was conducted on the individual mean RT recorded on trials associated with a correct response. The analysis revealed a main effect of load ($F(1, 10) = 33.2$; $p < .001$), reflecting longer RT in the load-4 condition (1151 ms) than in the load-2 condition (1040 ms). No other factor or interaction in this analysis were significant.

2.2.2. fNIRS

The fNIRS z -maps in the ipsilateral and contralateral conditions against baseline activation for Δ HbO are graphically illustrated in Fig. 3. Positive z values were also found for Δ HbT (see Table 1) but not for Δ HbR. Given that Δ HbT is the sum of Δ HbO and Δ HbR, the following analyses are focused on Δ HbO values.

As Fig. 3 suggests, the z -maps for the ipsilateral and contralateral conditions show a high degree of similarity. Δ HbO z -maps show a diffused neural activation extending over most of the regions investigated by the present optode placements. Δ HbO concentration values indicate that all investigated channels were active in both the ipsilateral and contralateral conditions. z -maxima were observed at B4/D4 (IPS–IOS), in both the ipsilateral ($z = 2.69$, $p < .05$) and contralateral ($z = 2.52$, $p < .05$) conditions. The other region that yielded high z values was sIPS, with $z = 2.51$ ($p < .05$) for A1/C1 in the contralateral condition and $z = 2.38$ ($p < .05$) for A2/C2 in the ipsilateral condition. This result indicates that both IPS–IOS and sIPS were strongly involved in the retention phase of the change-detection task.

Fig. 4 and Table 2 report the fNIRS results in the load-2 and load-4 conditions against baseline activation. As shown in the z -maps, all recording channels were significantly active in both the load-2 and load-4 conditions, with the z -maxima for Δ HbO localized at B4/D4 (IPS–IOS; $z = 2.42$, $p < .05$) in the load-2 condition, and at A1/C1 (sIPS; $z = 2.49$; $p < .05$) and B4/D4 (IPS–IOS; $z = 2.47$, $p < .05$) in the load-4 condition. Also in this case, the result suggests a strong involvement of both IPS–IOS and sIPS in the retention phase of the change-detection task.

The high similarity between the activation patterns found in the comparisons against baseline should not be surprising, because the analyses were intended to verify the involvement of the parieto-occipital circuit (and especially of IPS–IOS) in VSTM task. We therefore performed a set of finer-grained analyses based on hemodynamic responses computed by taking into account the individual differences in timing of peak activity (see Section 2). In the first step of these analyses, the new sets of individual optical maps for the contralateral and ipsilateral conditions were compared with a series of paired one-tail t -tests. The analyses indicated significantly higher concentration value in the contralateral condition relative to the ipsilateral condition restricted to B4/D4 (IPS–IOS; mean Δ HbO value in nM \pm SD of contralateral vs. ipsilateral trials: 197.06 ± 122.52 vs. 153.10 ± 102.16 ; $z = 2.87$, $p < .05$). The contrast z -map (contralateral minus ipsilateral) is illustrated in Fig. 5.

In order to quantify the lateralization effect at B4/D4 (IPS–IOS), effect sizes (d) were calculated following the algorithm adopted by Cohen (1988; for a practical example, see Schroeter, Cutini, Wahl, Scheid, & von Cramon, 2007), who derived d as the difference between the mean d value in the contralateral condition and the mean d value in the ipsilateral condition, divided by the mean

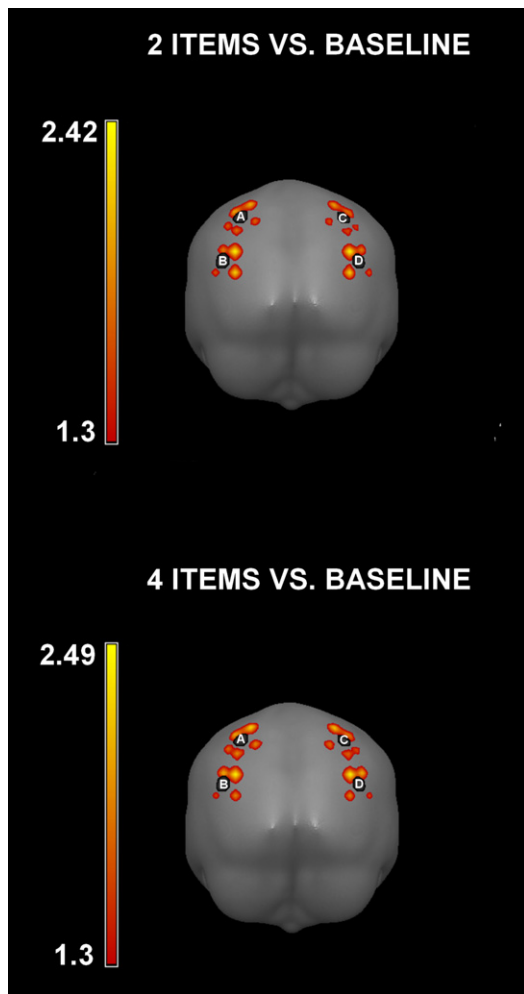


Fig. 4. Statistical (z) maps for ΔHbO of the load-2 condition vs. baseline comparison (upper panels) and load-4 condition vs. baseline comparison (lower panels). From left to right: occipital view and top view. The z -maps have been overlaid onto the ICBM152 brain template.

standard deviation of d values in the ipsilateral and contralateral conditions. Mean effect size was 0.41 at B4/D4 (IPS–IOS). We performed the same analysis on sIPS, although the contralateral vs. ipsilateral contrast was not significant. Mean effect sizes at A1/C1 and A2/C2 (left/right sIPS) were -0.15 and -0.03 , respectively, confirming that the lateralization effect is confined to IPS–IOS.

A second series of analyses was focused on the ROI showing a distinctive lateralized response, that is, IPS–IOS (B4/D4). Individual ΔHbO concentration and peak latency values in this region were calculated in each cell of design generated by the factorial combination of load and side (see Fig. 6, panels a and b). The resulting amplitude and latency values were submitted to separate ANOVAs considering load and side as within-subject factors. The ANOVA on ΔHbO concentration revealed a significant effect of side ($F(1, 10) = 7.72, p < .05$) and a significant effect of load ($F(1, 10) = 8.69, p < .05$), reflecting increased activation in the load-4 condition relative to the load-2 condition. The interaction between side and load was not significant ($F < 1$). The ANOVA on peak latencies revealed a marginal main effect of load ($F(1, 10) = 3.64, p < .086$), and no other significant effects.¹

¹ The use of a two-steps design in the analyses of the data estimated via the peak-based approach could raise the potential of the influence of double dipping (Kriegeskorte et al., 2009) or selection bias (Vul et al., 2009) in the results. This is

3. Discussion

The present study examined the behavioral and cortical hemodynamic responses of subjects engaged in the cued variant of a change-detection task using an fNIRS apparatus. Memory performance decreased and reaction time (RT) increased as memory load increased from two to four objects, suggesting that the mechanisms supporting the maintenance of information in VSTM were taxed to a larger extent as the number of remembered objects increased (Klaver et al., 1999; Todd & Marois, 2004; Vogel & Machizawa, 2004). Using fNIRS, a broader family of hemodynamic response parameters could be explored relative to fMRI (see Section 1). Despite the reduced spatial resolution with respect to fMRI, fNIRS could detect changes in ΔHbO (invisible to fMRI) concentration in the cortical blood flow with a higher sampling frequency. Although the hemodynamic response remains sluggish in comparison with the neuronal response, the higher sampling frequency of the response enabled us to measure the fine temporal structure of the response, and most importantly the time at which the response reached its peak. The hemodynamic results were clear-cut in indicating increased levels of ΔHbO concentration in the contralateral IPS–IOS relative to the ipsilateral condition. Furthermore, though attenuated with respect to the contralateral equivalent, the ipsilateral IPS–IOS region showed levels of ΔHbO concentration correlated with VSTM load much in the same way as found in the contralateral homologous area. On the temporal side, Fig. 6b suggests that activation of IPS–IOS, both contralaterally and ipsilaterally, also tended to be correlated with load, with an earlier hemodynamic responses elicited in the load-2 condition than in the load-4 condition.

In the current study, the information provided by ΔHbO variations was more reliable than that offered by HbT. Since HbT results from the sum of HbO and HbR, and the HbR signal quality obtained in the present study was clearly sub-optimal (i.e., no significant channel resulted significantly activated in random-effect analysis), we deemed appropriate to use only the HbO concentration for the more specific analysis on the interaction between load and lateralization. Although ΔHbO activation is thought to be less localized than HbT (Culver, Siegel, Franceschini, Mandeville, & Boas, 2005), recent investigations on neurovascular coupling (Berwick et al., 2008; Sirotin, Hillman, Bordier, & Das, 2009) showed that the half-width of ΔHbO is comparable to that of HbT. Furthermore, the value of the information contained in ΔHbO is confirmed by an elegant optical imaging investigation of the initial dip in alert monkeys (Sirotin et al., 2009). The initial dip consists in the observed initial darkening in intrinsic signal optical imaging (e.g., Chen-Bee, Agoncillo, Xiong, & Frostig, 2007), or in the temporarily reduced BOLD signal in fMRI (e.g., Menon et al., 1995). While the initial dip was usually interpreted as a local conversion of HbO to HbR caused by increased oxygen consumption by local neurons before any active vascular response (Frostig, Lieke, Ts'o, & Grinvald, 1990), Sirotin et al. (2009) have shown that the initial dip largely reflects increases in HbO (see also Sirotin & Das, 2010), with no significant increase in HbR. They argued that the initial dip occasionally found with fMRI is likely to contain no privileged information about neural activity, while blood volume (HbT) signal “is as rapid and spatially focused and more than an order of magnitude stronger

however highly unlikely in the present case, for the dataset used in the exploratory analyses comparing contralateral vs. ipsilateral activity was organized with different criteria with respect to those used in the analyses conducted on data estimated via the peak-based approach. While therefore the main effect of side in the ANOVA conducted on peak-latency amplitude values was redundant because it depended on the ROI selection criteria (i.e., only the ROIs showing a lateralized response were submitted to further analysis), there was no *a priori* reason to expect that hemodynamic activity at such ROIs would also be modulated by VSTM memory load.

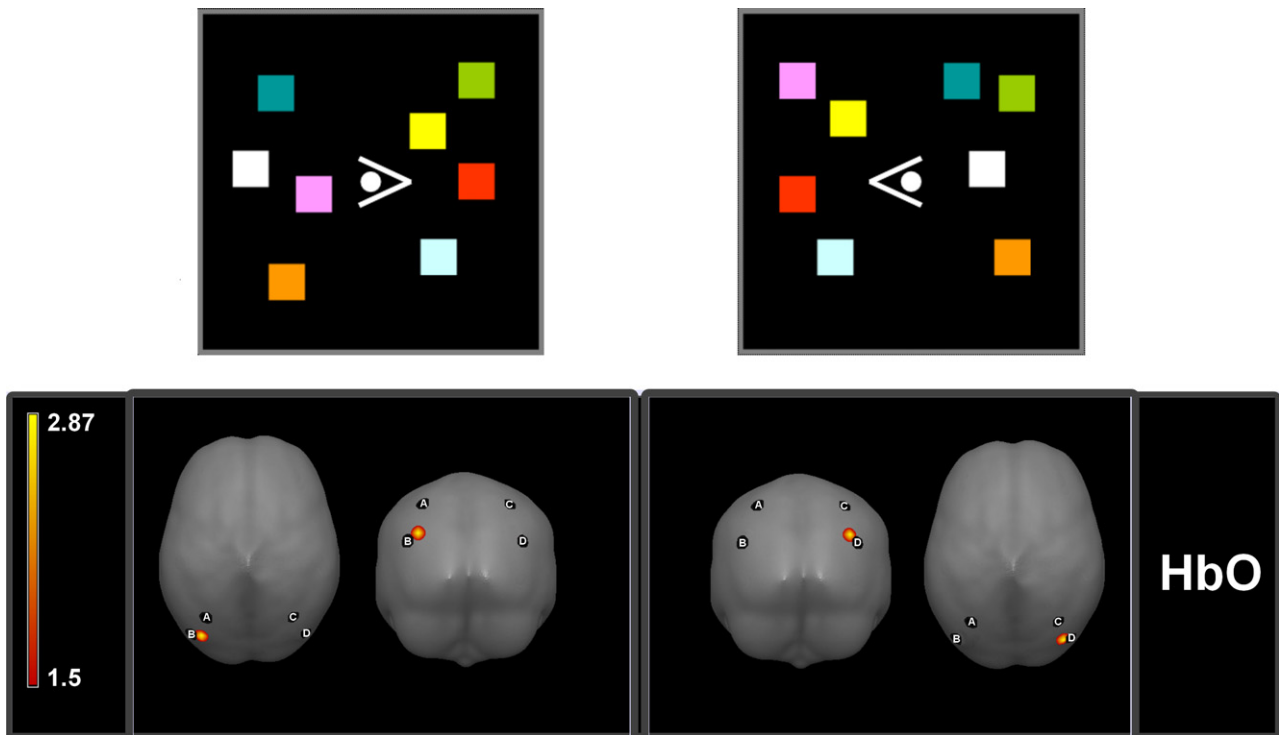


Fig. 5. Occipital and top views of the statistical (z) maps of contralateral vs. ipsilateral comparison for Δ HbO. The z -maps have been overlaid onto the ICBM152 brain template. For illustrative purposes, the upper part of the figure shows examples of memory arrays with the hemifields including the to-be-memorized colored squares (contralateral to the hemisphere where the enhanced concentration of HbO was observed in the present study) cued by arrow heads. Note however that colored squares and arrow heads were never displayed synchronously during the experiment (see Fig. 1).

and longer lived” (Sirotnin et al., 2009). Considering that HbT is the sum of HbO and HbR, it is conceivable to hypothesize that HbO can provide further information with respect to HbR (i.e., the BOLD response in fMRI).

We began our investigation with the observation that EEG and MEG results typically reveal a larger increase of electrical or magnetic field intensity with increasing memory load over the hemisphere contralateral to the side from which visual stimuli are encoded (Klaver et al., 1999; Vogel & Machizawa, 2004), but that this relationship had not been clearly established for hemodynamic correlates of neuronal activity. In this perspective, the present results are largely consistent with the findings of Robitaille

et al. (2010), in that the increase in Δ HbO concentration with increasing load in the present work was about the same for the contralateral and ipsilateral IOS–IPS. Robitaille et al. (2010) did find an enhanced contralateral response, but not one that correlated with observed memory performance. In a related paper (Robitaille et al., 2009) in which brain signals measured during the retention of visual stimuli were subjected to a wavelet transform, in order to examine the timecourse of induced oscillatory activity during memory retention, the dominant oscillatory component was in the alpha band. Interestingly, alpha-band activity increased in amplitude with increasing memory load and this increase had the same amplitude on the contralateral and ipsilateral sides (Grimault et al.,

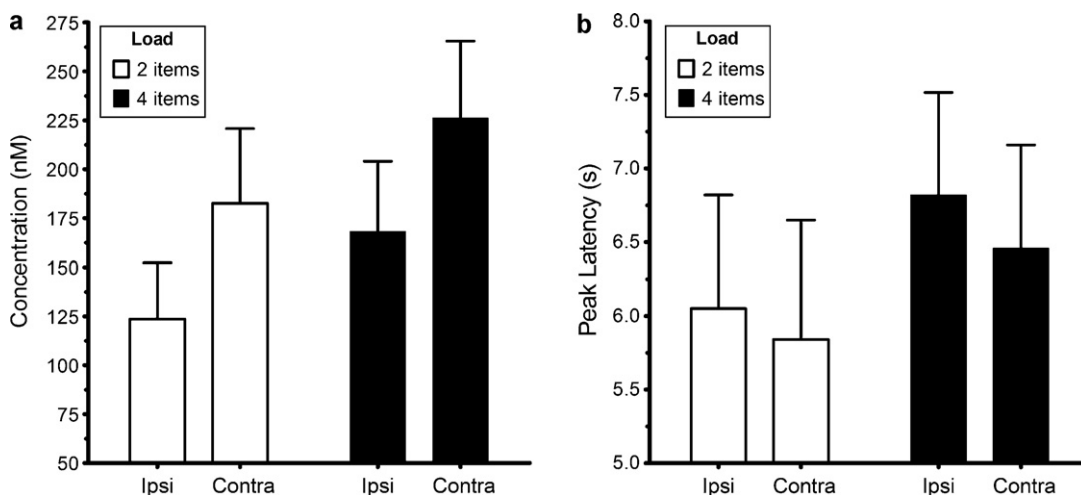


Fig. 6. Bar graph (mean and standard error) of Δ HbO activity (panel a) and peak latency (panel b) recorded at B4/D4 (IPS–IOS), graphed as a function of load and side (see text for details). The mean peak latency of the Δ HbO response profiles (following normalization of individual hemodynamic response in each cell of the side by load design) corresponds to the average time at which Δ HbO concentration reached the peak amplitude during the 10 s interval from onset.

2009). It is possible that the hemodynamic response is influenced by the amplitude of the oscillatory activity in the dominant oscillation mode (alpha-band), and given that alpha-band amplitude increases with memory load, hemodynamic measures would also tend to show the same relationship. One piece of information that is at odds with this possibility, however, is that the amplitude of alpha-band oscillations tends to be lower in the hemisphere contralateral to the encoded stimuli; but the amplitude of the hemodynamic response here was, on the contrary, larger on the contralateral side. The present results suggest, therefore, that the hemodynamic response is not likely to reflect, primarily, changes in alpha-band activity related to attention. The closer connection with effects found in memory suggests that fNIRS measures of ΔHbO may prove useful in future studies of the representation of objects in VSTM.

Different theoretical scenarios may be entertained herein to explain the discrepancy between a clearly lateralized response typically detected using the ERP approach (i.e., SPCN or CDA), and the bilateral activation of BOLD and MEG responses found by Robitaille et al. (2009, 2010) and confirmed in the present context using fNIRS. The worst case is a general lack of power in detecting what ultimately should have been reflected in an interaction between the two monitored factors, load and objects' lateralization. Although this could certainly be taken into account as a potential risk, the strict adherence between the present results and those of Robitaille et al. suggest we should consider other possibilities. One possibility entails the different timescales of the SPCN and hemodynamic reflections of the variable manipulated in our memory task. Whereas SPCN is usually visible in a 300–900 ms time-window (when the retention interval is not much longer and stimuli do not remain visible during the retention interval; see Drew & Vogel, 2008), the raise of BOLD and/or other hemodynamic functions is decidedly postponed, with the subtended risk that subtle effects found with one technique (unique as far as temporal resolution is concerned) cannot be found with other techniques monitoring different types of neural activity. In addition, the extended time-scale of hemodynamic effects when testing VSTM with change-detection designs makes it extremely difficult to isolate effects triggered by mental routines responsible for VSTM maintenance, and separate them from effects due to probe array processing. For instance, the present design, where VSTM load and item numerosity in the probe array were confounded lends itself to the obvious criticism that the observed hemodynamic results may have been inflated by the perceptual complexity of the probe array rather than reflecting, as we are trying to argue, VSTM load and retention. In this vein, the argument would be that as the perceptual complexity of the probe array was increased (from load-2 trials to load-4 trials), the comparison process between memory and probe array became more difficult (Awh, Barton, & Vogel, 2007), and this, rather than VSTM load at retention, would be the true modulatory factor of cortical hemodynamic variations that we reported.² Recent work on the

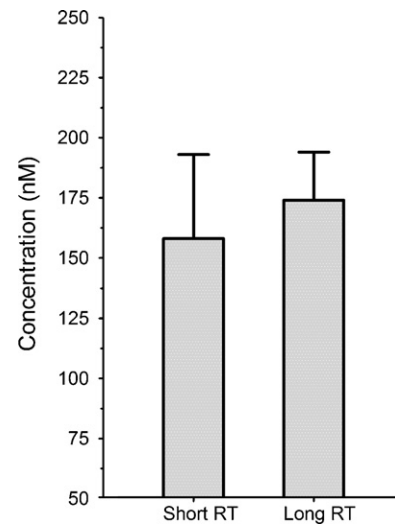


Fig. 7. Bar graph (mean and standard error) of ΔHbO activity recorded at B4/D4 (IPS-IOS), graphed as a function of RT in the change-detection task. Short RT, RT shorter than median RT (collapsed across memory-load levels). Long RT, RT longer than median RT (collapsed across memory-load levels).

comparison between perceptual input and VSTM content suggests that a direct reflection of the difficulty in comparing memory and probe arrays for detection of a change is an increase in RT as memory load – and probe array size – is increased (Hyun, Woodman, Vogel, Hollingworth, & Luck, 2009). The longer RT in the load-4 condition relative to RT in load-2 condition observed in the present empirical context would therefore be in line with the present argument. To check this alternative perspective we devised two tests in which the link between RT length in the change-detection task and ΔHbO peak-based concentration values recorded at IPS-IOS was parametrically estimated. RTs in the load-2 and load-4 conditions were first divided into long and short RTs (911 ms vs. 1280 ms; $F(1, 10) = 476.1, p < .001$) via median-split, and the corresponding mean ΔHbO values in contralateral IPS-IOS associated with each RT category were compared via *t*-test. As Fig. 7 makes particularly clear, the influence of RT length on the distribution of ΔHbO values recorded at IPS-IOS was nil ($t(10) = 0.63, p > .8$). In addition, an ANOVA on the same ΔHbO values considering load as factor and ΔRT (load-4 RT minus load-2 RT) as covariate revealed a significant effect of load ($F(1, 10) = 6.51, p < .05$), but no significant interaction between load and ΔRT ($F(1, 10) = 1.99, p > .5$). The results of these two tests suggest strongly that the processing subtended in the comparison between memory and probe arrays had a negligible impact on the hemodynamic results observed in this study.

A second explicative scenario is that the different techniques discussed here may be sensitive to different aspects of the processing subtended in visual information encoding and maintenance, or to the activity of different populations of neurons that cohabit in a relatively small portion of the cortex like IPS-IOS. We know too little at present about the cytoarchitectural properties of these neurons to exclude *tout-court* that a subpopulation of these neurons with specific properties (e.g., generating open-field potentials) may be also those whose VSTM-driven unbalanced ipsi- vs. contralateral activation would be visible to EEG, but not to fMRI, fNIRS, or MEG. It is intriguing indeed that even the technique closest to EEG, i.e., MEG, was not as sensitive to magnified VSTM load effects contralaterally to the encoding side as EEG usually is, despite analogous temporal resolution to EEG and similarity of the bio-signals monitored with these techniques (Robitaille et al., 2010).

Though quite tentative and demanding caution given the marginally significant effects, the temporal picture emerging from the present investigation, taken together with the amplitude

² There are other solutions that may have been adopted to circumvent the covariation between memory and probe array numerosity discussed in this section, one of which would have been to present in the probe array just a single colored square in one of the positions previously occupied by the colored squares in the memory array. It must be noted, however, that this solution is not devoid of problems when studying lateralization effects using a cued variant of a change-detection task. A probe array containing a single colored square is asymmetrical and the possibility that a contralateral response at the hemodynamic level may be exacerbated by this feature of the probe array is not negligible. Even presenting a single colored square centrally, so as to prevent a physical asymmetry in the probe display, would be sub-optimal, because of the known effects arising when the context (i.e., the spatial arrangement and relative position of the colored squares) of the memory array is disrupted by the probe array (e.g., by changing the spatial position of the color square subject to change between the memory and probe arrays; Jiang et al., 2000; Hyun et al., 2009).

results of ΔHbO concentration, is actually consistent with a particular observation often made when monitoring SPCN activity in the cued variant of the change-detection task. The present results indicated reduced ΔHbO concentration values ipsilaterally than contralaterally, independently of the difference in ΔHbO concentration values associated with the load-2 and load-4 conditions. The temporal parameters associated with ΔHbO variations over the monitored interval indicated faster ΔHbO responses in the load-2 condition than in the load-4 condition, both ipsilaterally and contralaterally. A typical observation when inspecting a SPCN component is that contralateral activation to memorized objects tends to remain stable in the mentioned 300–900 ms time-window, while ipsilateral activation becomes progressively less positive and ultimately converges to contralateral activation values. On the assumption that ipsilateral activation, at least temporarily shortly after the memory-array presentation, reflects inhibition of distractor information (i.e., of the to-be-ignored objects in the cued variant of the change-detection task), the emerging temporal/amplitude picture based on the present results allows one to speculate that inhibition is likely to be no longer necessary shortly after the offset of the memory-array, and that the VSTM system (at least the subroutines relying in IPS–IOS neural activity) may react more promptly when suppressing less information (in the load-2 condition) than more information (in the load-4 condition). This increase in reactivity is generally compatible with the notion that VSTM at capacity may work less efficiently relative to when the encoded information is below capacity, and may also account for the decrease in accuracy in the load-4 condition compared to the load-2 condition. On this account, a portion of the errors in detecting a change between memory and probe arrays in the load-4 condition would be attributed to the *delayed* inhibition of ipsilateral items when encoding objects from particularly crowded memory arrays. Note this is less trivial that it may seem at first blush if one considers redundancy gain dynamics. More explicitly, it is obvious that a larger population of inputs converges on IPS–IOS when there are four objects to encode in VSTM than when there are only two. Given the relatively large distance between our stimuli (relative to early receptive-field sizes) and the retinotopic organization of the visual system, each stimulus can be modeled as stimulating an independent channel. With more inputs, converging independent channels could have been expected to produce an earlier activation as the number of channels increases because the probability of a fast response increases as the number of channels increases (Logan, 1988; Miller, 1982). The temporal aspects of results just discussed suggest that redundancy gain is unlikely to influence the activity of neurons in IPS–IOS, although a replication of the present results, perhaps using a paradigm and/or fNIRS setting with a finer temporal resolution, is absolutely necessary before drawing firm conclusions about this particular aspect of the present results.

Acknowledgments

This work was supported by an ERC Grant (210922-GENMOD) and Compagnia San Paolo to M. Z., and by a PRIN Grant from the Italian Ministry of University (200888LWHZ) and a Cross-Area Grant from the University of Padova (CPDA098913) to R. D.'A.

References

- Aguirre, G. K., Zarahn, E., & D'Esposito, M. (1998). Neural components of topographic representation. *Proceedings of the National Academy of Sciences (USA)*, *95*, 839–846.
- Awh, E., Barton, B., & Vogel, E. K. (2007). Visual working memory represents a fixed number of items regardless of complexity. *Psychological Science*, *18*, 622–628.
- Beck, D. M., Rees, G., Frith, C. D., & Lavie, N. (2001). Neural correlates of change detection and change blindness. *Nature Neuroscience*, *4*, 645–650.
- Benjamini, Y., & Hochberg, Y. (1995). Controlling the false discovery rate: A practical and powerful approach to multiple testing. *Journal of the Royal Statistical Society: Series B*, *57*, 289–300.
- Berwick, J., Johnston, D., Jones, M., Martindale, J., Martin, C., Kennerley, A. J., et al. (2008). Fine detail of neurovascular coupling revealed by spatiotemporal analysis of the hemodynamic response to single whisker stimulation in rat barrel cortex. *Journal of Neurophysiology*, *99*, 787–798.
- Chelazzi, L., Miller, E. K., Duncan, J., & Desimone, R. (1993). A neural basis for visual search in inferior temporal cortex. *Nature*, *363*, 345–347.
- Chen-Bee, C. H., Agoncillo, T., Xiong, Y., & Frostig, R. D. (2007). The triphasic intrinsic signal: Implications for functional imaging. *Journal of Neuroscience*, *27*, 4572–4586.
- Cohen, J. (1988). *Statistical power analysis for the behavioral sciences* ((2nd ed.)). Hillsdale, NJ: Lawrence Erlbaum Associates.
- Cohen, J. D., Perlstein, W. M., Braver, T. S., Nystrom, L. E., Noil, D. C., Jonides, J., et al. (1997). Temporal dynamics of brain activation during a working memory task. *Nature*, *386*, 604–608.
- Coltheart, M. (1980). Iconic memory and visible persistence. *Perception & Psychophysics*, *27*, 183–228.
- Cope, M., & Delpy, D. T. (1988). System for long-term measurement of cerebral blood and tissue oxygenation on newborn infants by near infra-red transillumination. *Medical and Biological Engineering and Computing*, *26*, 289–294.
- Courtney, S. M., Ungerleider, L. G., Keil, K., & Haxby, J. V. (1997). Transient and sustained activity in a distributed neural system for human working memory. *Nature*, *386*, 608–611.
- Cowan, N. (2001). The magical number 4 in short-term memory: A reconsideration of mental storage capacity. *Behavioral and Brain Science*, *24*, 87–185.
- Culver, J. P., Siegel, A. M., Franceschini, M. A., Mandeville, J. B., & Boas, D. A. (2005). Evidence that cerebral blood volume can provide brain activation maps with better spatial resolution than deoxyhemoglobin. *NeuroImage*, *27*, 947–959.
- Cutini, S., Scatturin, P., & Zorzi, M. (2010). A new method based on ICBM152 head surface for probe placement in multichannel fNIRS. *NeuroImage*, *42*, 945–955.
- Cutini, S., Scatturin, P., Menon, E., Bisiacchi, P. S., Gamberini, L., Zorzi, M., et al. (2008). Selective activation of the superior frontal gyrus in task-switching: An event-related fNIRS study. *NeuroImage*, *42*, 945–955.
- Dell'Acqua, R., Sessa, P., Jolicoeur, P., & Robitaille, N. (2006). Spatial attention freezes during the attentional blink. *Psychophysiology*, *43*, 394–400.
- Devaraj, A., (2005). Signal Processing for functional near-infrared neuroimaging. Unpublished MS Thesis. Drexel University.
- Drew, T., & Vogel, E. K. (2008). Neural measures of individual differences in selecting and tracking multiple moving objects. *Journal of Neuroscience*, *28*, 4183–4191.
- Duncan, A., Meek, J. H., Clemence, M., Elwell, C. E., Fallon, P., Tyszczyk, L., et al. (1996). Measurement of cranial optical path length as a function of age using phase resolved near infrared spectroscopy. *Pediatric Research*, *39*, 889–894.
- Franceschini, M. A., Toronov, V., Filiaci, M. E., Gratton, E., & Fantini, S. (2000). On-line optical imaging of the human brain with 160-ms temporal resolution. *Optics Express*, *6*, 49–57.
- Frostig, R. D., Lieke, E. E., Ts'o, D. Y., & Grinvald, A. (1990). Cortical functional architecture and local coupling between neuronal activity and the microcirculation revealed by in vivo high-resolution optical imaging of intrinsic signals. *Proceedings of the National Academy of Sciences of the United States of America*, *87*, 6082–6086.
- Crimault, S., Robitaille, N., Grova, C., Lina, J.-M., Dubarry, A.-S., & Jolicoeur, P. (2009). Oscillatory activity in parietal and dorsolateral prefrontal cortex during retention in visual short-term memory: Additive effects of spatial attention and memory load. *Human Brain Mapping*, *30*, 3378–3392.
- Grubbs, F. E. (1969). Procedures for detecting outlying observations in samples. *Technometrics*, *11*, 1–21.
- Harrison, A., Jolicoeur, P., & Marois, R. (2010). 'What' and 'where' in the intraparietal sulcus: An fMRI study of object identity and location in visual short-term memory. *Cerebral Cortex*, *20*, 2478–2485.
- Huppert, T. J., Hoge, R. D., Diamond, S. G., Franceschini, M. A., & Boas, D. A. (2006). A temporal comparison of BOLD, ASL, and NIRS hemodynamic responses to motor stimuli in adult humans. *NeuroImage*, *29*, 368–382.
- Hyun, J.-s., Woodman, G. F., Vogel, E. K., Hollingworth, A., & Luck, S. J. (2009). The comparison of visual working memory representations with perceptual inputs. *Journal of Experimental Psychology: Human Perception and Performance*, *35*, 1140–1160.
- Ikkay, A., McCollough, A. W., & Vogel, E. K. (2010). Contralateral delay activity provides a neural measure of the number of representations in visual working memory. *Journal of Neurophysiology*, *103*, 1963–1968.
- Irwin, D. E., Brown, J. S., & Sun, J. (1988). Visual masking and visual integration across saccadic eye movements. *Journal of Experimental Psychology: General*, *117*, 276–287.
- Jack, A. I., Patel, G. H., Astafiev, S. V., Snyder, A. Z., Akbudak, E., Shulman, G. L., et al. (2007). Changing human visual field organization from early visual to extra-occipital cortex. *PLoS ONE*, *5*, e452.
- Jiang, Y., Olson, I. R., & Chun, M. M. (2000). The organization of visual short-term memory. *Journal of Experimental Psychology: Learning, Memory, and Cognition*, *26*, 683–702.
- Johnson, S. J., Spencer, J. P., Luck, S. J., & Schöner, G. (2009). A dynamic neural field model of visual working memory and change detection. *Psychological Science*, *20*, 568–577.

- Jolicœur, P., Brisson, B., & Robitaille, N. (2008). Dissociation of the N2pc and sustained posterior contralateral negativity in a choice response task. *Brain Research*, 1215, 160–172.
- Jolicœur, P., Sessa, P., Dell'Acqua, R., & Robitaille, N. (2006a). On the control of visual spatial attention: Evidence from human electrophysiology. *Psychological Research*, 70, 414–424.
- Jolicœur, P., Sessa, P., Dell'Acqua, R., & Robitaille, N. (2006b). Attentional control and capture in the attentional blink paradigm: Evidence from human electrophysiology. *European Journal of Cognitive Psychology*, 18, 560–578.
- Klaver, P., Talsma, D., Wijers, A. A., Heinze, H.-J., & Mulder, G. (1999). An event-related brain potential correlate of visual short-term memory. *NeuroReport*, 10, 2001–2005.
- Kriegeskorte, N., Simmons, W. K., Bellgowan, P. S., & Baker, C. I. (2009). Circular analysis in systems neuroscience: The dangers of double dipping. *Nature Neuroscience*, 12, 535–540.
- Lefebvre, C., Jolicœur, P., & Dell'Acqua, R. (2010). Electrophysiological evidence of enhanced cortical activity in the human brain during visual curve tracing. *Vision Research*, 50, 1321–1327.
- Logan, G. D. (1988). Toward an instance theory of automatization. *Psychological Review*, 95, 492–527.
- Luck, S. J., & Vogel, E. K. (1997). The capacity of visual working memory for features and conjunctions. *Nature*, 390, 279–281.
- Luria, R., Sessa, P., Gotler, A., Jolicœur, P., & Dell'Acqua, R. (2009). Visual short-term memory capacity for simple and complex objects. *Journal of Cognitive Neuroscience*, 22, 496–512.
- Maki, A., Yamashita, Y., Watanabe, E., & Koizumi, H. (1996). Visualizing human motor activity by using non-invasive optical topography. *Frontiers of Medical and Biological Engineering*, 7, 285–297.
- McCollough, A. W., Machizawa, M. G., & Vogel, E. K. (2007). Electrophysiological measures of maintaining representations in visual working memory. *Cortex*, 43, 77–94.
- Menon, R. S., Ogawa, S., Hu, X., Strupp, J. P., Anderson, P., & Ugurbil, K. (1995). BOLD based functional MRI at 4T includes a capillary bed contribution: Echo-planar imaging correlates with previous optical imaging using intrinsic signals. *Magnetic Resonance in Medicine*, 33, 453–459.
- Miller, J. O. (1982). Divided attention: Evidence for coactivation with redundant signals. *Cognitive Psychology*, 14, 247–279.
- Mitchell, D., & Cusack, R. (2008). Flexible, capacity-limited activity of posterior parietal cortex in perceptual as well as visual short-term memory tasks. *Cerebral Cortex*, 18, 1788–1798.
- Nee, D. E., & Jonides, J. (2009). Common and distinct neural correlates of perceptual and memorial selection. *NeuroImage*, 45, 963–975.
- Nuwer, M. R., Comi, G., Emerson, R., Fuglsang-Frederiksen, A., Guerit, J. M., Hinrichs, H., et al. (1998). IFCN standards for digital recording of clinical EEG. *Electroencephalography and Clinical Neurophysiology*, 106, 259–261.
- Okamoto, M., Dan, H., Sakamoto, K., Takeo, K., Shimizu, K., Kohno, S., et al. (2004). Three-dimensional probabilistic anatomical cranio-cerebral correlation via the international 10–20 system oriented for transcranial functional brain mapping. *NeuroImage*, 21, 99–111.
- Perron, R., Lefebvre, C., Robitaille, N., Brisson, B., Gosselin, F., Arguin, M., et al. (2009). Attentional and anatomical considerations for the representation of simple stimuli in visual short-term memory: Evidence from human electrophysiology. *Psychological Research*, 73, 222–232.
- Pessoa, K., Gutierrez, E., Bandettini, P. A., & Ungerleider, L. G. (2002). Neural correlates of visual working memory: fMRI amplitude predicts task performance. *Neuron*, 35, 975–987.
- Phillips, W. A. (1974). On the distinction between sensory storage and short-term visual memory. *Perception & Psychophysics*, 16, 283–290.
- Predovan, D., Prime, D., Arguin, M., Gosselin, F., Dell'Acqua, R., & Jolicœur, P. (2009). On the representation of words and nonwords in visual short-term memory: Evidence from human electrophysiology. *Psychophysiology*, 46, 191–199.
- Prime, D., Dell'Acqua, R., Arguin, M., Gosselin, F., Jolicœur, P. (2010). Spatial layout of letters in nonwords affects visual short-term memory load: Evidence from human electrophysiology. *Psychophysiology*, in press.
- Prime, D. J., & Jolicœur, P. (2009). Mental rotation requires visual short-term memory: Evidence from human electric cortical activity. *Journal of Cognitive Neuroscience*, 22, 2437–2446.
- Rensink, R. A. (2000a). The dynamic representation of scenes. *Visual Cognition*, 7, 17–42.
- Rensink, R. A. (2000b). Visual search for change: A probe into the nature of attentional processing. *Visual Cognition*, 7, 345–376.
- Robitaille, N., Grimault, S., & Jolicœur, P. (2009). Bilateral parietal and contralateral responses during the maintenance of unilaterally encoded objects in visual short-term memory: Evidence from magnetoencephalography. *Psychophysiology*, 46, 1090–1099.
- Robitaille, N., Marois, R., Todd, J., Grimault, S., Cheyne, D., & Jolicœur, P. (2010). Distinguishing between lateralized and nonlateralized brain activity associated with visual short-term memory: fMRI, MEG, and EEG evidence from the same observers. *NeuroImage*, 53, 1334–1345.
- Rouder, J. N., Morey, R. D., Cowan, N., Zwilling, C. E., Morey, C. C., & Pratte, M. S. (2008). An assessment of fixed-capacity models of visual working memory. *Proceedings of the National Academy of Sciences (USA)*, 105, 5975–5979.
- Sato, H., Kiguchi, M., Kawaguchi, F., & Maki, A. (2004). Practicality of wavelength selection to improve signal-to-noise ratio in near-infrared spectroscopy. *NeuroImage*, 21, 1554–1562.
- Saults, J. S., & Cowan, N. (2007). A central capacity limit to the simultaneous storage of visual and auditory arrays in working memory. *Journal of Experimental Psychology: General*, 136, 663–684.
- Savitzky, A., & Golay, M. J. E. (1964). Smoothing and differentiation of data by simplified least squares procedures. *Analytical Chemistry*, 36, 1627–1639.
- Scarpa, F., Cutini, S., Scatturin, P., Dell'Acqua, R., & Sparacino, G. (2010). Bayesian filtering of human brain hemodynamic activity elicited by visual short-term maintenance recorded through functional near-infrared spectroscopy (fNIRS). *Optic Express*, 18, 26550–26558.
- Schroeter, M. L., Zysset, S., Kruggel, F., & von Cramon, D. Y. (2003). Age-dependency of the hemodynamic response as measured by functional near-infrared spectroscopy. *NeuroImage*, 19, 555–564.
- Schroeter, M. L., Cutini, S., Wahl, M. M., Scheid, R., & von Cramon, D. Y. (2007). Neurovascular coupling is impaired in cerebral microangiopathy: An event-related Stroop study. *NeuroImage*, 34, 26–34.
- Sereno, M. I., Pitzalis, S., & Martinez, A. (2001). Mapping of contralateral space in retinotopic coordinates by a parietal cortical area in humans. *Science*, 294, 1350–1354.
- Singh, A., Okamoto, M., Dan, H., Jurcak, V., & Dan, I. (2005). Spatial registration of multichannel multi-subject fNIRS data to MNI space without MRI. *NeuroImage*, 27, 842–851.
- Sirotin, Y. B., Hillman, E. M., Bordier, C., & Das, A. (2009). Spatiotemporal precision and hemodynamic mechanism of optical point spreads in alert primates. *Proceedings of the National Academy of Sciences of the United States of America*, 106, 18390–18395.
- Sirotin, Y. B., & Das, A. (2010). Reply to Uludağ: fMRI initial dip reflects increase in oxygenated hemoglobin. *Proceedings of the National Academy of Sciences of the United States of America*, 107, E24.
- Song, J. H., & Jiang, Y. V. (2006). Visual working memory for simple and complex features: An fMRI study. *NeuroImage*, 20, 963–972.
- Strangman, G., Culver, J. P., Thompson, J. H., & Boas, D. A. (2002). A qualitative comparison of simultaneous BOLD fMRI and NIRS recordings during functional brain activity. *NeuroImage*, 17, 719–731.
- Thériault, M., De Beaumont, L., Tremblay, S., Lassonde, M., Jolicœur, P. (2010). Cumulative effects of concussions in athletes revealed by electrophysiological abnormalities in visual working memory. *Journal of Clinical and Experimental Neuropsychology*, in press.
- Todd, J. J., & Marois, R. (2004). Capacity limit of visual short-term memory in human posterior parietal cortex. *Nature*, 428, 751–754.
- Villringer, A., Planck, J., Hock, C., Schleinkofer, L., & Dirnagl, U. (1993). Near infrared spectroscopy (NIRS): A new tool to study hemodynamic changes during activation of brain function in human adults. *Neuroscience Letters*, 154, 101–104.
- Vogel, E. K., & Machizawa, M. G. (2004). Neural activity predicts individual differences in visual working memory capacity. *Nature*, 428, 748–751.
- Vogel, E. K., McCollough, A. W., & Machizawa, M. G. (2005). Neural measures reveal individual differences in controlling access to working memory. *Nature*, 438, 500–503.
- Vogel, E. K., Woodman, G. F., & Luck, S. J. (2001). Storage of features, conjunctions, and objects in visual working memory. *Journal of Experimental Psychology: Human Perception and Performance*, 27, 92–114.
- Vul, E., Harris, C., Winkielman, P., & Pashler, H. (2009). Puzzlingly high correlations in fMRI studies of emotion, personality, and social cognition. *Perspectives in Psychological Science*, 4.
- Wheeler, M. E., & Treisman, A. M. (2002). Binding in short-term memory. *Journal of Experimental Psychology: General*, 131, 48–64.
- Xu, Y., & Chun, M. M. (2006). Dissociable neural mechanisms supporting visual short-term memory for objects. *Nature*, 440, 91–95.
- Yamamoto, T., & Kato, T. (2002). Paradoxical correlation between signal in functional magnetic resonance imaging and deoxygenated hemoglobin content in capillaries: A new theoretical explanation. *Physics in Medicine and Biology*, 47, 1121–1141.
- Zeki, S. M. (1993). *A vision of the brain*. Oxford, UK: Blackwell Scientific Publications.